Numerical investigation of particle formation mechanisms in silane discharges

Kathleen De Bleecker,* Annemie Bogaerts, and Renaat Gijbels
Department of Chemistry, University of Antwerp, Universiteitsplein 1, 2610 Wilrijk, Belgium

Wim Goedheer
FOM-Institute for Plasma Physics "Rijnhuizen," P.O. Box 1207, 3430 BE Nieuwegein, The Netherlands
(Received 24 December 2003; published 26 May 2004)

The formation of particles in low-pressure silane discharges has been studied extensively over the last decade. In this paper we try to identify, by numerical simulations, the precursors of the dust formation and we examine the gas-phase reactions leading to larger clusters, and finally to nanometer or micrometer sized particles. A one-dimensional fluid model is used, which incorporates silicon hydrides (Si_nH_m) containing up to 12 silicon atoms. A set of 68 species, including neutrals, radicals, ions, and electrons, is taken into account. The importance of various cluster reaction sequences is discussed. Besides the discussion of ion-molecule and ion-ion reactions, the role of the vibrationally excited silane molecules and of SiH_3 radicals on the particle growth process is studied. Finally, the effect of temperature variation on the density of the dust particles is investigated.

DOI: 10.1103/PhysRevE.69.056409 PACS number(s): 52.27.Lw

I. INTRODUCTION

Hydrogenated amorphous silicon (a-Si:H) thin films are commonly produced by plasma enhanced chemical vapor deposition (PECVD) and have been the subject of a lot of research over the last decade [1–4]. Apart from being used in the fabrication of thin film solar cells [5–7] a-Si:H has also an extensive field of applications in other devices, i.e., thin film transistors used in liquid crystal displays [8,9], light emitting diodes [10,11], etc. Nanoparticle formation, causing the creation of "dusty plasmas," is a generally recognized problem in PECVD, especially when trying to achieve high deposition rates with good layer quality. Initially the dust grains were solely considered harmful, because they contaminated the substrate. In the microelectronics industry, particles with diameters as small as tens of nanometers may cause killer defects [12,13]. Therefore, the research primarily aimed at avoiding the particle formation and/or contamination. Since then this field has been rapidly expanding. It appears that film deposition in solar cells application now even benefits from the presence of nanoparticles [14]. It was found that if particles were deposited in the films, while their size was still small (order of a few nanometers), the films show improved properties [15,16]. The so-called polymorphous silicon thin films have superior electronic properties leading to solar cells that show stability against light induced defect creation—thus making this material a good candidate for use in high-efficiency solar cells [13,17].

Good knowledge of the plasma species densities (electrons, positive and negative ions, various molecules, radicals, as well as dust particles) together with a good understanding of their behavior in the discharge can assist in the design and optimization of the equipment and the processes. It can assist in eliminating undesirable contaminants, as well as create new ways for generating desirable particles for enhanced film properties. However, despite the widespread use of PECVD processes and the fact that deposition of silicon from silane is one of the best studied PECVD systems, the details of the chemistry occurring during deposition and especially of the nanoparticles formation are not yet well understood.

In this paper the initial step of particulate growth in a dust forming silane discharge is investigated. Based on experiments [18], the nucleation appears to take place by a series of chemical reactions, better known as gas-phase polymerization. Starting from silane, larger silicon hydrides are formed and can finally lead to hydrogenated silicon clusters that can be considered as dust particles.

Several recent publications have dealt with this issue [19–21]. Gallagher [19,20] presented a simple homogeneous plasma-chemistry model where particles primarily grow from SiH_3^- anions and SiH_m radicals, first into $Si_xH_m^-$ ions and Si_xH_m radicals, which then grow into silicon hydride particles. Gallagher mainly focuses on the calculation of electron, ion, radical, and silane collisions with $Si_xH_m^z$ radicals and ions with z charges. Realistic estimates of the radical and cation densities are used [20]. Bhandarkar *et al.* [21] developed a zero-dimensional chemical kinetic nucleation model in which linear and cyclic silicon hydride species containing up to ten silicon atoms were considered. They assume a constant positive ion density (proportional to the rf power) and use it as an input parameter.

When studying particle nucleation and growth in a discharge, it is important that the model accounts self-consistently for the coupling between particle growth and changes of the plasma properties. In contrast to the studies performed so far we make use of a one-dimensional fluid model, where the electron kinetics, the chemistry of the discharge, as well as the deposition process are described in a self-consistent way. The electron kinetics (electron impact reactions, electron transport coefficients) depend strongly on the electron energy distribution function (EEDF). In contrast

*Electronic address: kathleen.debleecker@ua.ac.be

to Ref. [21], the EEDF is not assumed to be Maxwellian, since it can often deviate significantly [22], and is influenced by the composition of the background gas. The EEDF is calculated by solving the Boltzmann equation in a two-term approximation and is used to create a look-up table for the electron rate coefficients and transport coefficients as a function of the average electron energy. In a previous study we developed an initial model for the description of the dust formation [23].

The main reason for using a one-dimensional (1D) model is the reduction of the computational effort compared to higher-dimensional models, while the spatial transport due to gradients is still taken into account. The 1D model can be applied to carry out a sensitivity study of the relevance of certain chemical reactions in the plasma. Since this is here our main concern, the 1D approach is the best option.

Various theories address the clustering mechanism in silane discharges. In general there are three possible routes to consider, involving either positive ion, neutral, and negative ion reaction pathways. The cation route seems the less likely option, since a kinetic bottleneck is already formed at clusters having relatively low numbers of silicon atoms, preventing clustering reactions beyond five or six silicon atoms. This has been extensively investigated by Mandich *et al.* [24]. Moreover, the positive ions are efficiently evacuated from the plasma across the sheaths, resulting in insufficient time for a cation to undergo an entire clustering reaction sequence. Watanabe *et al.* [25,26], who studied the neutral clustering pathway, argue that SiH_2 insertion reactions play an important role in the formation of bigger particles. Nonetheless, most authors consider the main pathway leading to clustering to be governed by anion-neutral reactions [19–21,27–29]. The long residence time of the anions in the plasma, electrically confined by the plasma sheaths, favors their further growth, and makes them good candidates to trigger particle nucleation. Mass spectra, measured by Hollenstein *et al.* [30], show a good correlation between the anions and particle formation. Once the particles are formed, they can grow further by coagulation and, eventually, due to deposition of radicals or ions on the particle surface.

In our calculations, dust is primarily formed by successive reactions of anions with silane molecules. Exact data for the rate constants of these anion-molecule reactions are still not known. Therefore a comparison is made between two situations where the rates of these reactions are varied, according to data known from literature. In this paper we will also focus on the role of vibrationally excited silane molecules and of SiH_3 radicals on the particle growth process. Compared with ground state silane, vibrationally excited silane can in fact enhance the kinetics of the clustering mechanism. A study of their contribution is made for the different clustering situations. Besides silane, the radical SiH_3 can also play a role in the early stages of particle formation if the rate of the radical-anion reactions is much higher than the rate of anion-molecule reactions. In this model anions containing up to a maximum of 12 silicon atoms are incorporated; hence, no reactions are included that lead to the formation of $Si_nH_m^-$ with $n>12$.

In Sec. II we describe the fluid model and the mechanisms for particle growth. In Sec. III simulation results of the initial step of particle formation are presented and the influence of variation of certain parameters (e.g., rate constants, temperature) on the densities of the dust particles is studied. Conclusions are presented in Sec. IV.

II. MODEL DESCRIPTION

A. Fluid model

In our 1D fluid model the discharge is described by particle balance equations for the ions, electrons, and neutrals, and an energy balance equation for the electrons. The electric field is calculated from the Poisson equation, which is coupled to the balance equations, making the model fully self-consistent. Power input into the plasma is transferred to the charged species (electrons and ions) by ohmic heating.

The fluid model for describing a silane/hydrogen discharge was originally developed by Nienhuis *et al.* [31,32]. In the present paper, this model is used to investigate the nucleation of dust in a silane plasma. The most important aspects of the model will be given here. Further details concerning the numerical techniques and algorithms can be found in Refs. [33,34]. Typical discharge quantities, such as the fluxes, densities of the particles, and the electric field, are calculated self-consistently.

The density balance for each species j (electrons, ions, radicals, and neutral molecules) is described by

$$\frac{dn_j}{dt} + \frac{d\Gamma_j}{dx} = S_j, \tag{1}$$

where n_j and Γ_j are the particle's density and flux, respectively, and S_j represents the different source and sink terms of particle j (respectively, formation/destruction). The gas inlet and pumping have been incorporated by the introduction of additional source and sink terms. The chemically inert molecules are perfectly mixed over the entire reactor volume. The radicals, on the other hand, can undergo reactions/transitions at the wall, resulting in a nonuniform profile.

The momentum balance is replaced by a drift-diffusion approximation, which means that each particle flux consists of two separate terms, a drift and a diffusion term,

$$\Gamma_j = \mu_j n_j E - D_j \frac{dn_j}{dx}, \tag{2}$$

where μ_j and D_j are the mobility and diffusion coefficient of species j, and E represents the electric field. The diffusion coefficient of the positive and negative ions is obtained from the Einstein relation (see Sec. II D). For the neutral particles the mobility term is equal to zero. Equation (2) assumes that the charged particles will react instantaneously to a change in the electric field. Because the ions cannot follow the actual electric field, an effective electric field is taken into account which compensates the inertia effects originating from their lower momentum transfer frequency. An expression for the effective electric field is obtained by neglecting the diffusive transport and inserting the expression $\Gamma_i = \mu_i n_i E_{eff}$ in the simplified momentum balance:

TABLE I. Overview of the different species incorporated in the model, besides the electrons.

Molecules	Ions	Radicals
SiH_4, $SiH_4^{(2-4)}$, $SiH_4^{(1-3)}$	SiH_3^+, $Si_2H_4^+$	SiH_3, SiH_2
H_2	H_2^+	H
	SiH_3^-, SiH_2^-	
Si_2H_6, Si_3H_8, Si_4H_{10}, Si_5H_{12}	$Si_2H_5^-$, $Si_3H_7^-$, $Si_4H_9^-$, $Si_5H_{11}^-$	Si_2H_5, Si_3H_7, Si_4H_9, Si_5H_{11}
Si_6H_{14}, Si_7H_{16}, Si_8H_{18}, Si_9H_{20}	$Si_6H_{13}^-$, $Si_7H_{15}^-$, $Si_8H_{17}^-$, $Si_9H_{19}^-$	Si_6H_{13}, Si_7H_{15}, Si_8H_{17}, Si_9H_{19}
$Si_{10}H_{22}$, $Si_{11}H_{24}$, $Si_{12}H_{26}$	$Si_{10}H_{21}^-$, $Si_{11}H_{23}^-$, $Si_{12}H_{25}^-$	$Si_{10}H_{21}$, $Si_{11}H_{23}$, $Si_{12}H_{25}$
	$Si_2H_4^-$, $Si_3H_6^-$, $Si_4H_8^-$, $Si_5H_{10}^-$	Si_2H_4, Si_3H_6, Si_4H_8, Si_5H_{10}
	$Si_6H_{12}^-$, $Si_7H_{14}^-$, $Si_8H_{16}^-$, $Si_9H_{18}^-$	Si_6H_{12}, Si_7H_{14}, Si_8H_{16}, Si_9H_{18}
	$Si_{10}H_{20}^-$, $Si_{11}H_{22}^-$, $Si_{12}H_{24}^-$	$Si_{10}H_{20}$, $Si_{11}H_{22}$, $Si_{12}H_{24}$

$$\frac{d\Gamma_i}{dt} = \frac{en_i}{m_i}E - \nu_{m,i}\Gamma_i, \tag{3}$$

where $\nu_{m,i}$ is the momentum transfer frequency of the ion i given by

$$\nu_{m,i} = \frac{e}{\mu_i\, m_i}. \tag{4}$$

Here e represents the elementary charge and m_i the mass of the ion. The effective electric field, replacing the instantaneous electric field in Eq. (2), is then given by

$$\frac{d\Gamma_{eff,i}}{dt} = \nu_{m,i}(E - E_{eff,i}). \tag{5}$$

The electric field E and the potential V are calculated using the Poisson equation,

$$\frac{d^2V}{dx^2} = -\frac{e}{\epsilon_0}\left(\sum n_+ - \sum n_- - n_e\right), \quad E = -\frac{dV}{dx}, \tag{6}$$

where ϵ_0 is the permittivity of free space, n_e the electron density, n_+ the total positive ion density, and n_- the total negative ion density (the negative dust species included).

The electron energy density $w_e = n_e\epsilon$ (i.e., the product of the electron density and the average electron energy) is calculated self-consistently from the second moment of the Boltzmann equation,

$$\frac{dw_e}{dt} + \frac{d\Gamma_w}{dx} = -e\Gamma_e E + S_w, \tag{7}$$

with Γ_w the electron energy density flux,

$$\Gamma_w = \frac{5}{3}\mu_e w_e E - \frac{5}{3}D_e\frac{dw_e}{dx}, \tag{8}$$

and μ_e and D_e are the electron mobility and electron diffusion coefficient. The term S_w in Eq. (7) represents the loss of electron energy due to electron impact collisions. No energy balance is included for the ions and neutrals. The energy dissipated by the ions is only accounted for in the overall energy balance of the discharge, where a preset total consumed power is specified.

B. Plasma kinetics

In order to model the formation of dust in a silane discharge, the 1D silane model, developed by Nienhuis *et al.* [31], has been extended with chemical reactions leading to the formation of bigger particles. Since particle nucleation is at this point our main interest, we have included silicon hydrides containing up to a maximum of 12 silicon atoms and we try to identify the precursors of the dust formation. We will especially focus on the role of the plasma-activated vibrational excitation of SiH_4, and also on the role of the SiH_3 radicals.

1. Species included in the model

An overview of the different species (molecules, ions, and radicals) taken into account in our model is given in Table I. In addition to silane ground state molecules, vibrationally excited silane molecules, formed by electron impact collision on ground state silane, are also considered. The first vibrational levels of silane $SiH_4^{(2-4)}$, i.e., the bending modes at 0.113 eV, and $SiH_4^{(1-3)}$, i.e., the stretching modes at 0.271 eV, are therefore incorporated as separate species.

For every saturated silane molecule Si_nH_{2n+2}, the corresponding Si_nH_{2n+1} radical has to be considered, since hydrogen abstraction is an important reaction in silane plasmas. The silylenes Si_nH_{2n} are also included, since their corresponding anions play a role in the initial particle formation. The silylenes are a reactive form of the silenes (i.e., molecules containing a double bond between two silicon atoms). They are characterized by a single bond between the two silicon atoms with two nonbonding electrons. Through isomerization reactions, the silylenes can be altered to the thermodynamically more stable silenes. The silenes themselves are, however, not incorporated in the present model because of their unreactive nature. While the positive ions are limited to SiH_3^+, $Si_2H_4^+$, and H_2^+, the negative ions are extended up to species containing 12 silicon atoms. We make a distinction between the silyl anions ($Si_nH_{2n+1}^-$) and the silylene anions ($Si_nH_{2n}^-$), as will be explained in the following paragraphs.

2. Electron collisions

Some chemical reactions require an energy threshold and are initiated by electrons, which have typically a mean ki-

TABLE II. The electron collisions used in the model, with the reference where their cross sections are taken from.

S. No.	Reaction	Threshold energy (eV)	Reaction-type	Reference
1	$SiH_4+e^-\rightarrow SiH_3^++H+2e^-$	11.9	Dissociative ionization	[35]
2	$SiH_4^{(2-4)}+e^-\rightarrow SiH_3^++H+2e^-$	11.8	Dissociative ionization	[35]
3	$SiH_4^{(1-3)}+e^-\rightarrow SiH_3^++H+2e^-$	11.7	Dissociative ionization	[35]
4	$Si_2H_6+e^-\rightarrow Si_2H_4^++2H+2e^-$	10.2	Dissociative ionization	[35]
5	$SiH_4^{(0)}+e^-\rightarrow SiH_4^{(2-4)}+e^-$	0.11	Vibrational excitation	[36]
6	$SiH_4^{(0)}+e^-\rightarrow SiH_4^{(1-3)}+e^-$	0.27	Vibrational excitation	[36]
7	$SiH_4+e^-\rightarrow SiH_3+H+e^-$	8.3	Dissociation	[37,38]
8	$SiH_4^{(2-4)}+e^-\rightarrow SiH_3+H+e^-$	8.2	Dissociation	[37,38]
9	$SiH_4^{(1-3)}+e^-\rightarrow SiH_3+H+e^-$	8.1	Dissociation	[37,38]
10	$SiH_4+e^-\rightarrow SiH_2+2H+e^-$	8.3	Dissociation	[37,38]
11	$SiH_4^{(2-4)}+e^-\rightarrow SiH_2+2H+e^-$	8.2	Dissociation	[37,38]
12	$SiH_4^{(1-3)}+e^-\rightarrow SiH_2+2H+e^-$	8.1	Dissociation	[37,38]
13	$Si_2H_6+e^-\rightarrow SiH_3+SiH_2+H+e^-$	7.0	Dissociation	[37]
14	$SiH_4+e^-\rightarrow SiH_3^-+H$	5.7	Dissociative attachment	[39]
15	$SiH_4^{(2-4)}+e^-\rightarrow SiH_3^-+H$	5.6	Dissociative attachment	[39]
16	$SiH_4^{(1-3)}+e^-\rightarrow SiH_3^-+H$	5.5	Dissociative attachment	[39]
17	$SiH_4+e^-\rightarrow SiH_2^-+2H$	5.7	Dissociative attachment	[39]
18	$SiH_4^{(2-4)}+e^-\rightarrow SiH_2^-+2H$	5.6	Dissociative attachment	[39]
19	$SiH_4^{(1-3)}+e^-\rightarrow SiH_2^-+2H$	5.5	Dissociative attachment	[39]
20	$H_2+e^-\rightarrow H_2^++2e^-$	15.4	Ionization	[40]
21	$H_2+e^-\rightarrow H_2^{(v=1)}+e^-$	0.54	Vibrational excitation	[41]
22	$H_2+e^-\rightarrow H_2^{(v=2)}+e^-$	1.08	Vibrational excitation	[41]
23	$H_2+e^-\rightarrow H_2^{(v=3)}+e^-$	1.62	Vibrational excitation	[41]
24	$H_2+e^-\rightarrow H+H+e^-$	8.9	Dissociation	[42]

netic energy of a few eV. Electron impact on SiH_4 is responsible for the production of radicals, ions, and molecules. An overview of the different electron collisions (ionization, dissociation, attachment, and vibrational excitation) with their respective threshold energies and references for the cross sections is presented in Table II. The cross sections of the electron collisions for SiH_4, Si_2H_6, and H_2 are given in Fig. 1, where the number of the curves corresponds to the number of the electron collisions shown in Table II. The EEDF is calculated from the Boltzmann equation in the two-term approximation, and is needed to calculate, from the above cross sections, the rate constants of the electron impact collisions, which are expressed as a function of average electron energy.

Dissociation of SiH_4 leads mostly to the formation of SiH_3 and SiH_2 radicals with a branching ratio of 0.17/0.83, in favor of SiH_2 [37].

The ionization cross sections for SiH_4 and Si_2H_6 have been measured by Krishnakumar *et al.* [35]. All the ionization cross sections are lumped and linked to the ion which is most likely formed. So we only consider SiH_3^+, $Si_2H_4^+$, and H_2^+ as the ionization products of SiH_4, Si_2H_6, and H_2, respectively.

Dissociative attachment cross sections for SiH_4 are obtained from Haaland [39]. Similarly to the lumping of the ionization cross sections, only SiH_3^- and SiH_2^- are considered as the most important anions formed from the dissociative attachment of SiH_4, with over 70% leading to the formation of SiH_3^-. As can be seen from Fig. 1, the cross section for the formation of SiH^- by dissociative attachment (represented by curve *a*) is so low that this species is not taken into account separately. Si^- is also a minor product and could not even be detected in the measurements of Haaland [39,43]. The cross sections for the formation of SiH_3^- and SiH_2^- by dissociative attachment are not particularly large. Indeed, they are two orders of magnitude lower than the corresponding dissociative ionization cross sections. However, dissociative attachment represents the most important source of negative ions in the silane plasma, and the residence time for negative ions in the discharge is longer compared to that of any other species. Even modest production rates of anions can lead to a substantial buildup of the anions, as they are electrically confined by the plasma sheaths. Hence, mutual anion-cation neutralization represents the only loss process for the negative ions (see below).

Dissociative attachment on Si_2H_6 leads to the production of both disilicon anions $Si_2H_m^-(m=0-5)$ and monosilicon anions $SiH_m^-(m=0-3)$ [44]. Rate constants were derived from the dissociative attachment cross sections of SiH_4 and Si_2H_6

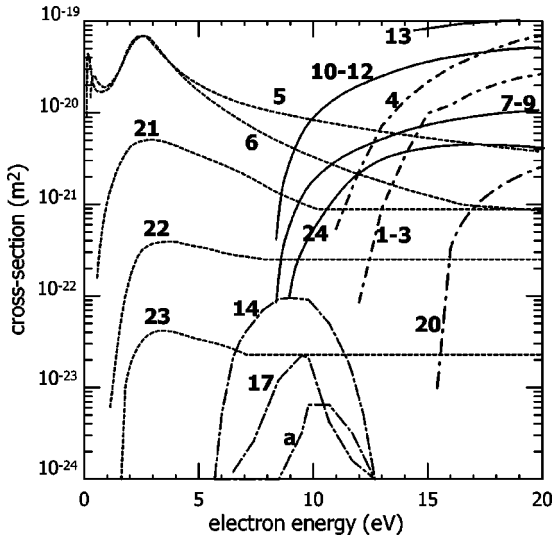

FIG. 1. Cross sections of the electron collisions with SiH_4, Si_2H_6, and H_2 taken into account in our model. The numbers of the curves correspond to the numbers of the reactions shown in Table II. Curve *a* represents the production of SiH^- through dissociative attachment of SiH_4 and is not included in our model because the cross section is very low. The dissociative attachment of vibrationally excited SiH_4 molecules is described by curves 14 and 17, multiplied by a factor 10 (see text).

by Perrin *et al.* [27], by integrating over a Maxwellian energy distribution. For $T_e=3$ eV, the rate constant for Si_2H_6 is at most three times larger than that for SiH_4. But despite this enhanced attachment, the Si_2H_6 concentration represents only a few percent of the gas mixture, and our calculations show that the production of anions through this pathway is negligible in comparison to the dissociative attachment of SiH_4, and therefore dissociative attachment on Si_2H_6 is not considered. The same applies for the dissociative attachment on larger silicon hydrides.

The anion H^-, is not considered either, since, for its production to be significant, it first requires the production of excited H_2 molecules, which can then undergo dissociative attachment leading to the formation of H^- ($e^-+H_2^* \rightarrow H+H^-$). Indeed, in the particular case of H_2, the dissociative attachment cross section increases more than one order of magnitude per additional vibrational quantum [45]. Because of the constraint of two successive reactions and the loss of excited H_2 molecules due to quenching at the walls, the calculated density of H^- proved to be insignificant in our calculations.

The vibrational excitation cross sections of SiH_4 are characterized by a steep threshold at the vibrational energies followed by a steep drop and a second maximum, as shown in Fig. 1. Vibrational excitation by electron impact is an important process to consider in our calculations, since the vibrationally excited SiH_4 molecules ($SiH_4^{(2-4)}$ and $SiH_4^{(1-3)}$) can play an essential role in the primary stage of particle formation. Furthermore, these cross sections also account for a major energy loss for the electrons.

Similar to ground state silane, vibrationally excited SiH_4 molecules can also undergo ionization, dissociation, and dissociative attachment, but data for their cross sections were difficult to find. Therefore, for the ionization and dissociation, the cross sections of ground state silane have been used as an approximation, with its threshold shifted to lower electron energy (see Table II). A reasonable increase in the dissociative attachment cross section for the vibrationally excited SiH_4 can be expected, since it is stated in Ref. [46] that the vibrationally and rotationally excited molecules can drastically increase the dissociative attachment. Therefore, we have increased the cross sections of ground state SiH_4 for the formation of SiH_3^- and SiH_2^- (curves 14 and 17 in Fig. 1) by an order of magnitude, and we have shifted the respective threshold to lower electron energy.

In contrast to SiH_4, the vibrationally excited species of H_2 (H_2^ν with $\nu=1-3$) are treated as ground state H_2, in order to reduce the number of species. However, their respective vibrational excitation has been included in the model, to properly calculate the electron energy. Their separate incorporation is also not required to take the increased dissociative attachment cross section into account, as the production of H^- still remained negligible in the present calculations (see above).

3. Ion-molecule and molecule-molecule reactions: General aspects

In Tables III and IV the important ion-molecule and molecule-molecule reactions are summarized. The rate constants in the tables reflect the values at a gas temperature of 400 K and a gas pressure of 0.3 Torr or 40 Pa (p_0 is denoted in Pa units in the tables). Some of the rates are a function of gas temperature or pressure and their general notation is given in the comment section of the table. Reactions 1–9 in Table III are part of a "standard" silane/hydrogen discharge, i.e., without the integration of dust, and form the basis for the further extension of our model, namely, to include the initial phase of dust formation. A further detailed discussion of the chemical reactions in Table III can be found in Ref. [31]. Here we will focus our attention on the gas-phase reactions leading to larger clusters and consider reactions between silicon hydrides containing up to 12 silicon atoms (see Table IV). In the following sections the different aspects of the anion chemistry are discussed.

4. Anion-molecule reactions: Cluster growth

Since the silicon hydride anions are electrostatically trapped in the plasma bulk, they can easily undergo polymerization reactions. The earliest stages of particle formation start primarily from the anions SiH_3^- and SiH_2^-, principally formed through the dissociative attachment of SiH_4 (reactions 14–19 of Table II).

The dominant negative ion, SiH_3^-, is the first species of the particle formation and can in turn undergo the following anion-molecule chain reactions:

$$SiH_3^- + SiH_4 \rightarrow Si_2H_5^- + H_2, \tag{9a}$$

$$Si_2H_5^- + SiH_4 \rightarrow Si_3H_7^- + H_2, \tag{9b}$$

$$\vdots$$

TABLE III. Basic ion-molecule and molecule-molecule reactions. The abbreviation "est" stands for estimated.

S.No.	Reaction	Rate constant ($m^3\ s^{-1}$)	Comment	Reference
Hydrogen abstraction				
1	$SiH_4+H\rightarrow SiH_3+H_2$	1.2×10^{-18}	$2.8\times10^{-17}\ [\exp(-1250/T_{gas})]$	[43,47]
2	$Si_2H_6+H\rightarrow Si_2H_5+H_2$	7.0×10^{-18}	$1.6\times10^{-16}\ [\exp(-1250/T_{gas})]$	[43,47]
3	$Si_2H_6+H\rightarrow SiH_3+SiH_4$	3.5×10^{-18}	$0.8\times10^{-16}\ [\exp(-1250/T_{gas})]$	[43,47]
4	$Si_nH_{2n+2}+H\rightarrow Si_nH_{2n+1}+H_2$	1.1×10^{-17}	$2.4\times10^{-16}\ [\exp(-1250/T_{gas})]$ $n=3,\ldots,12$	[43], est.
Cluster growth through SiH_2 insertion				
5	$SiH_2+H_2\rightarrow SiH_4$	2.7×10^{-20}	$3.0\times10^{-18}[1-(1+2.3\times10^{-4}p_0)^{-1}]$[a]	[43]
6	$SiH_2+SiH_4\rightarrow Si_2H_6$	2.3×10^{-17}	$2.0\times10^{-16}[1-(1+0.0032\ p_0)^{-1}]$[a]	[43]
7	$SiH_2+Si_nH_{2n+2}\rightarrow Si_{n+1}H_{2n+4}$	4.9×10^{-17}	$4.2\times10^{-16}[1-(1+0.0033p_0)^{-1}]$[a] $n=2,\ldots,11$	[43]
Other neutral-neutral reactions				
8	$Si_2H_5+Si_2H_5\rightarrow Si_4H_{10}$	1.5×10^{-16}		[43], est.
9	$SiH_3+SiH_3\rightarrow SiH_2+SiH_4$	1.5×10^{-16}		[43,48]

[a] p_0 in Pa units.

TABLE IV. Additional molecule-molecule and ion-molecule reactions taken into account in the model.

S. No.	Reaction	Rate constant ($m^3\ s^{-1}$)	Comment	Reference
Cluster growth through silyl anions ($Si_nH^-_{2n+1}$) with SiH_4, $SiH_4^{(2-4)}$, and $SiH_4^{(1-3)}$				
1	$Si_nH^-_{2n+1}+SiH_4\rightarrow Si_{n+1}H^-_{2n+3}+H_2$	1.0×10^{-18}	Expt. $n=1,\ldots,11$	[27]
2	$Si_nH^-_{2n+1}+SiH_4^{(2-4)}\rightarrow Si_{n+1}H^-_{2n+3}+H_2$	2.6×10^{-17}	$10^{-18}\times\exp[+(0.113\ \text{eV})/RT]$	[27], calc.
3	$Si_nH^-_{2n+1}+SiH_4^{(1-3)}\rightarrow Si_{n+1}H^-_{2n+3}+H_2$	1.0×10^{-15}	$10^{-18}\times\exp[+(0.271\ \text{eV})/RT]$ $n=1,\ldots,11$	[27], calc.
Cluster growth through silylene anions ($Si_nH^-_{2n}$) with SiH_4, $SiH_4^{(2-4)}$, and $SiH_4^{(1-3)}$				
4	$Si_nH^-_{2n}+SiH_4\rightarrow Si_{n+1}H^-_{2n+2}+H_2$	1.0×10^{-18}	Expt. $n=1,\ldots,11$	[27]
5	$Si_nH^-_{2n}+SiH_4^{(2-4)}\rightarrow Si_{n+1}H^-_{2n+2}+H_2$	2.6×10^{-17}	$10^{-18}\times\exp[+(0.113\ \text{eV})/RT]$	[27], calc.
6	$Si_nH^-_{2n}+SiH_4^{(1-3)}\rightarrow Si_{n+1}H^-_{2n+2}+H_2$	1.0×10^{-15}	$10^{-18}\times\exp[+(0.271\ \text{eV})/RT]$ $n=1,\ldots,11$	[27], calc.
Deexcitation of vibrationally excited SiH_4				
7	$SiH_4^{(2-4)}+SiH_4\rightarrow 2SiH_4$	1.0×10^{-18}	Calculated by interpolation (see text)	[49]
8	$SiH_4^{(1-3)}+SiH_4\rightarrow 2SiH_4$	1.2×10^{-18}	Calculated by interpolation (see text)	[49]
9	$SiH_4^{(2-4)}+H_2\rightarrow SiH_4+H_2$	3.7×10^{-18}	Calculated by interpolation (see text)	[49]
10	$SiH_4^{(1-3)}+H_2\rightarrow SiH_4+H_2$	4.1×10^{-18}	Calculated by interpolation (see text)	[49]
Neutralization reactions of silyl and silylene anions with SiH_3^+ and $Si_2H_4^+$				
11	$Si_nH^-_{2n+1}+SiH_3^+\rightarrow Si_nH_{2n+1}+SiH_3$	$\sim10^{-14}$	Calc. $n=1,\ldots,12$	[50]
12	$Si_nH^-_{2n+1}+Si_2H_4^+\rightarrow Si_nH_{2n+1}+2SiH_2$	$\sim10^{-14}$	Calc. $n=1,\ldots,12$	[50]
13	$Si_nH^-_{2n}+SiH_3^+\rightarrow Si_nH_{2n}+SiH_3$	$\sim10^{-14}$	Calc. $n=1,\ldots,12$	[50]
14	$Si_nH^-_{2n}+Si_2H_4^+\rightarrow Si_nH_{2n}+2SiH_2$	$\sim10^{-14}$	Calc. $n=1,\ldots,12$	[50]
Cluster growth through anion-SiH_3 reactions				
15	$Si_nH^-_m+SiH_3\rightarrow Si_{n+1}H^-_{m+1}+H_2$	1.0×10^{-15}	Not included in standard model $n=1,\ldots,11$	[27]

$$Si_nH_{2n+1}^- + SiH_4 \rightarrow Si_{n+1}H_{2n+3}^- + H_2, \quad (9c)$$

leading to the formation of larger silyl anions. The enthalpies of reaction of the first four steps in the clustering process are, respectively, $-0.07, +0.07, +0.07$, and 0.00 eV. According to Fridman *et al.* [51] this thermoneutral and even slightly endothermic nature of some reactions from the chain would result in an intermolecular energy barrier and even a kinetic bottleneck. This energy barrier can, however, be overcome by molecules carrying sufficient internal energy, i.e., the vibrationally excited silane molecules, which will be discussed later on in the following section.

A similar reaction sequence can occur starting from SiH_2^-:

$$SiH_2^- + SiH_4 \rightarrow Si_2H_4^- + H_2, \quad (10a)$$

$$Si_2H_4^- + SiH_4 \rightarrow Si_3H_6^- + H_2, \quad (10b)$$

$$\vdots$$

$$Si_nH_{2n}^- + SiH_4 \rightarrow Si_{n+1}H_{2n+2}^- + H_2, \quad (10c)$$

resulting in the formation of larger silylene anions, and thus represent a second important reaction chain.

A major problem is the poor knowledge of the corresponding reaction rate constants. A theoretical upper limit for the ion-molecule rate is given by the Langevin collision rate. The constant of the Langevin collision rate is given by [43]

$$k_L = e\left(\frac{\pi}{\epsilon_0}\right)^{1/2}\left(\frac{\alpha}{m_r}\right)^{1/2}, \quad (11)$$

where m_r represents the reduced mass in atomic mass units of the two reacting species and α is the neutral atom or molecule polarizability (in $Å^3$). The Langevin rate constant represents in any case an upper limit of the actual rate constant. Therefore Bhandarkar *et al.* [21] have reduced the Langevin rate constants by an order of magnitude, which results, in our case, in rate constants of the order of 10^{-16} m^3 s^{-1}(k_{g1}) [21,23]. On the other hand, Perrin *et al.* [27] predict that, based on conclusions derived from mass spectra, the rate constants of the anion-silane reactions are of the order of 10^{-18} m^3 s^{-1}(k_{g2}), so two orders of magnitude lower than the rate constants suggested by Bhandarkar. In Sec. III B we will compare both cases, but for our standard model we have used the rate constants suggested by Perrin.

As opposed to $Si_nH_{2n+1}^-$ and $Si_nH_{2n}^-$, the bare Si_n^- and Si_nH^- cluster anions seem to be very unreactive towards SiH_4. Perrin *et al.* suggest an upper limit for the reaction rate constant of about 10^{-19}m^3 s^{-1} (for $n \leqslant 7$) [27]. This low reactivity is attributed to the increase in electron affinity A_e for H-diluted or H-bare anions, resulting in a lack of exothermic channels towards SiH_4.

In theory, other anion-molecule reactions can occur. Reactions of anions with larger silanes (Si_nH_{2n+2} with $n>1$), e.g., $SiH_3^- + Si_2H_6 \rightarrow Si_3H_7^- + H_2$, are however not taken into account, since the density of Si_2H_6, and especially that of higher order silanes, is much lower than the SiH_4 density (at the most a few percent), making their contribution negligible.

5. Role of vibrationally excited $SiH_4^{(2-4)}$ and $SiH_4^{(1-3)}$ molecules

The rates of the anion-neutral reactions will be enhanced by the vibrationally excited molecules $SiH_4^{(2-4)}$ and $SiH_4^{(1-3)}$ Both species can likewise undergo anion-SiH_4^* reactions,

$$Si_nH_{2n+1}^- + SiH_4^* \rightarrow Si_{n+1}H_{2n+3}^- + H_2 \quad \text{for the silyl anions}, \quad (12)$$

and

$$Si_nH_{2n}^- + SiH_4^* \rightarrow Si_{n+1}H_{2n+2}^- + H_2 \quad \text{for the silylene anions}, \quad (13)$$

where SiH_4^* comprises both $SiH_4^{(2-4)}$ and $SiH_4^{(1-3)}$ (see reactions 2–3 and 5–6 in Table IV). The rate constants for the anion-SiH_4^* reactions are calculated based on the rate constant of the anion–ground state SiH_4 reaction (k_g),

$$k_g^* = k_g \exp\left(+\frac{E_{excess}}{RT_{gas}}\right). \quad (14)$$

We increased k_g by an exponential factor, containing the extra internal energy carried by the vibrationally excited molecules, which is 0.113 eV for $SiH_4^{(2-4)}$ and 0.271 eV for $SiH_4^{(1-3)}$, respectively. In this way we account for their lower activation energy E_a in the Arrhenius equation,

$$k_A = A \exp\left(-\frac{E_a}{RT_{gas}}\right), \quad (15)$$

where A represents a temperature independent constant. In the case of k_g equal to 10^{-18}m^3 s^{-1} (k_{g2}), k_g^* is typically 2.6×10^{-17} m^3 s^{-1} for $SiH_4^{(2-4)}$ and 2.6×10^{-15} m^3 s^{-1} for $SiH_4^{(1-3)}$, for a gas temperature of 400 K. The rate constant k_g^* cannot, however, exceed the Langevin rate constant (since it represents an upper limit), hence a maximum rate constant of 1.0×10^{-15} m^3 s^{-1} is adopted for $SiH_4^{(1-3)}$ (see reactions 3 and 6 of Table IV). For $k_g = 10^{-16}$ m^3 s^{-1}(k_{g1}), both $SiH_4^{(2-4)}$ and $SiH_4^{(1-3)}$ have a rate constant of 1.0×10^{-15} m^3 s^{-1}.

Evidently the deexcitation of the vibrationally excited molecules has to be incorporated. Besides their decay at the wall to ground state silane (incorporated by a 100% reaction chance in the reaction probability), deexcitation in the gas phase due to collisions with ground state silane and hydrogen has been considered (reactions 7–10 of Table IV). The reaction rate constants in the table represent the values at a gas temperature of 400 K, whereby H_2 appears to be the most efficient collision partner. In Perrin *et al.* [43] the deexcitation rate constant k_{deex} is derived for gas temperatures of 295 K and 500 K. The weak temperature dependence for collisions with ground state SiH_4 can be approximated by a linear interpolation of the values at 295 K and 500 K to obtain the reaction rate constants at 400 K [49]. This same temperature dependence has also been used for the deexcitation due to collisions with H_2.

6. Investigation of the importance of other production processes of SiH_3^-, beside dissociative attachment on SiH_4

The production of the initial SiH_3^- could be enhanced by the additional contribution of the fast H^- reaction [27],

$$H^- + SiH_4 \rightarrow SiH_3^- + H_2, \quad k = 5 \times 10^{-16}\ m^3\ s^{-1}. \quad (16)$$

But as mentioned above, the production of H^- requires two successive reactions (i.e., first vibrationally excited H_2 has to be formed, before significant dissociative attachment can take place) leading to a negligible production of H^-, and hence this process will not cause any extra production of SiH_3^- in the present calculations.

Another mechanism of initial SiH_3^- production comprises nondissociative electron attachment of SiH_3 radicals ($SiH_3 + e^- \rightarrow SiH_3^-$). Fridman *et al.* [51] predict that for relatively small particles (under 2 nm), the probability of electron nondissociative attachment will be small. The authors explain that this is due to the adiabatic nature of the energy transfer. The electron attachment will, however, strongly increase with cluster size, and it will become important for clusters exceeding the 2 nm size.

So we can conclude that the electron induced dissociative attachment on SiH_4 will be the main initial source of negative ions in our plasma and that nondissociative attachment reactions will become significant only for bigger silicon hydrides than the ones included in our model.

7. Anion-radical reactions

Anion-radical reactions can become important in a silane plasma, if the reactivity of the anions towards the radicals is much higher than their reactivity towards SiH_4. The most abundant silyl radical in the discharge, SiH_3, has in our calculations a steady-state concentration about three orders of magnitude lower than the concentration of SiH_4. This means that the anion-radical reactions have to proceed at a much higher rate constant than the anion-molecule reactions in order to be important in our model. Perrin *et al.* [27] predict that these exothermic reactions proceed at Langevin rate constant of the order of $10^{-15}\ m^3\ s^{-1}$. Hence, depending on the rate constant assumed for the anion-molecule reactions ($k_{g1} = 10^{-16}\ m^3\ s^{-1}$ suggested by Bhandarkar, or $k_{g2} = 10^{-18}\ m^3\ s^{-1}$ predicted by Perrin, see above), the anion-radical reactions can or cannot play a role in the initial phase of particle formation. In the results section the role of the radicals for the case of the assumed k_{g2} ($10^{-18}\ m^3\ s^{-1}$) is investigated.

It is important to mention that these reactions will lead to the dehydrogenation of the anion, as H_2 molecules are eliminated,

$$SiH_3^- + SiH_3 \rightarrow Si_2H_4^- + H_2, \quad (17a)$$

$$Si_2H_4^- + SiH_3 \rightarrow Si_3H_5^- + H_2, \quad (17b)$$

$$\vdots$$

$$Si_nH_m^- + SiH_3 \rightarrow Si_{n+1}H_{m+1}^- + H_2. \quad (17c)$$

A similar reaction pathway can be produced for SiH_2^-. It is clear from the above reactions that we would have to include a much higher number of different species, containing an even lower number of hydrogen atoms or no hydrogen at all (e.g., anions containing three silicon atoms would range from $Si_3H_7^-$ to $Si_3H_4^-$). All these new species can in turn undergo anion-molecule and anion-radical reactions, making the modeling of all the reactions impossible, especially if we also want to investigate the bigger anions. Consequently, if we want to investigate the role of the radicals in the clustering process, we do not make any distinction between silicon hydride molecules having the same number of silicon atoms, but different numbers of hydrogen atoms. The particle formation would then start from SiH_m^- with m comprising anions having three to zero hydrogen atoms. This mechanism is represented by reaction 15 in Table IV. In the results section the radical-anion reactions are investigated in a separate paragraph, where no distinction is made between the silyl and silylene anions, as opposed to the standard model.

Finally, charge transfer reactions between anions and radicals, e.g., $Si_nH_m^- + SiH_3 \rightarrow Si_nH_m + SiH_3^-$ can only occur if the radical has a higher electron affinity than the parent radical anion, since these reactions are energetically favored. Even though these reactions almost proceed at Langevin rate constant ($\approx 1.4 \times 10^{-16}\ m^3\ s^{-1}$), their contribution is neglected in our present calculations, due to the much lower concentration of the radicals in comparison to that of SiH_4.

8. Loss mechanisms for anions

Since the anions remain trapped by the positive plasma potential of the discharge, the only loss processes for the silyl and silylene anions are mutual anion-cation neutralization and electron detachment.

a. Mutual anion-cation neutralization. The main loss mechanism, by which the chain reaction of cluster growth is stopped, is the mutual anion-cation neutralization. The monomeric cation SiH_3^+ is the most abundant positive ion in the plasma. Reactions of silyl anions and silylene anions with SiH_3^+ lead to a charge exchange (reactions 11 and 13 in Table IV),

$$SiH_3^+ + Si_nH_{2n+1}^- \rightarrow SiH_3 + Si_nH_{2n+1}, \quad (18)$$

$$SiH_3^+ + Si_nH_{2n}^- \rightarrow SiH_3 + Si_nH_{2n}. \quad (19)$$

Besides SiH_3^+, $Si_2H_4^+$ is also taken into account for anion-cation neutralization (reactions 12 and 14 in Table IV). Although H_2^+ represents the third positive ion in our calculations, the concentration of this ion proves to be too low (see Sec. III) to take any part in the current mechanism and it is therefore not considered.

Hickman derived a semiempirical formula for the calculation of the mutual neutralization rate constant k_N between cations and anions [50],

$$k_N \approx (5.34 \times 10^{-13}) A_e^{-0.4} m_r^{-0.5} \left(\frac{T_{gas}}{300} \right)^{-0.5} (\mathrm{m^3\ s^{-1}}), \quad (20)$$

with A_e the electron affinity (in eV) of the parent neutral species of the anion, m_r the reduced mass (in amu), and T_{gas} the gas temperature in kelvin. Electron affinity data are taken from Ref. [52], where *ab initio* methods have been used to calculate the corresponding A_e. The electron affinity seems to slowly increase with the number of Si atoms, hence k_N will slightly decrease from typically $k_N \approx 1 \times 10^{-13}$ $\mathrm{m^3\ s^{-1}}$ for SiH_m^- to $k_N \approx 5 \times 10^{-14}$ $\mathrm{m^3\ s^{-1}}$ for $Si_{12}H_m^-$ for collisions with SiH_3^+ ($m=2n+1$ for the silyl anions and $m=2n$ for the silylene anions).

As an alternative, anion-cation association with or without the elimination of excess H or H_2 has been suggested by Haaland [39] and Bhandarkar *et al.* [21],

$$SiH_3^+ + Si_nH_m^- \rightarrow Si_{n+1}H_{m+3-y} + yH. \quad (21)$$

However, our model calculations predict that this type of reaction does not seem to contribute to the formation of larger silicon hydrides at the conditions under study (i.e., the concentrations of the larger species remained quasiunaffected when this process was included), and hence we have adopted the charge exchange mechanism instead of the association mechanism, because the rate constants are assumed the same [27].

b. Electron detachment from anions. Anions can only undergo electron detachment when the energy of the colliding species exceeds the electron affinity A_e of the parent neutral of the anion. The electron impact detachment, as well as the detachment due to collisions with excited species, is discussed below.

Electron impact detachment on ground state anion clusters $Si_nH_m^-$ can occur when $E_e > A_e$ (i.e., the electron affinity of the corresponding neutral),

$$e^-(E_e > A_e) + Si_nH_m^- \rightarrow 2e^- + Si_nH_m. \quad (22)$$

Because of their similar charge, the colliding electron has to overcome an additional repulsive Coulomb potential. The Coulomb potential describes the interaction between two point charges,

$$U = \frac{q_1 q_2}{4\pi\epsilon_0 r_{12}}, \quad (23)$$

where r_{12} is the distance between the anion and the electron, q_1 and q_2 the electric charge carried by the anion and the electron, respectively, and ϵ_0 is the permittivity of vacuum. Estimations from this equation, taking the interdistance parameter r_{12} in the order of 1 Å and assuming that the anion has one negative charge, result in a Coulomb potential of about 14 eV. Hence, electron impact detachment can only be important if the EEDF possesses a high energy tail in the distribution. However, we also have to bear in mind that, in our situation, the electron density n_e is almost two orders of magnitude lower than the positive ion density due to the presence of the anions. Hence, for small negative ions the mutual ion-ion neutralization will largely dominate over electron impact detachment. If we go to larger silicon hydrides, the rate of neutralization will gradually drop as m_r increases [see Eq. (20) above], whereas the rate of electron detachment increases with increasing size of the anion. Hence, ultimately the detachment could take over, but this applies only to larger clusters than the ones considered in our present model.

Collisional detachment of the anions by the excited species,

$$X^*(E^* > A_e) + Si_nH_m^- \rightarrow e^- + Si_nH_m + X, \quad (24)$$

takes place if the excited species carries enough internal energy. An estimation of the possible reaction rate is obtained by the following:

$$k_d = A \exp\left(-\frac{E_a}{RT_{gas}} \right) = \sigma_{ij}^2 \sqrt{\frac{8kT}{\pi m_r}} \exp\left(-\frac{E_a}{RT_{gas}} \right), \quad (25)$$

where m_r is the reduced mass, $\sigma_{ij} = (\sigma_i + \sigma_j)^{1/2}$ is the binary collision diameter in Å, E_a is the activation energy in J/mol, R is the universal gas constant, and T_{gas} is the gas temperature in kelvin. If we take the threshold energy for neutralizing SiH_3^- (1.4 eV) as an estimation for the value of activation energy, the rate constant of k_d would be of the order of 10^{-34} $\mathrm{m^3\ s^{-1}}$ for ground state colliding species, making this kind of reaction highly unlikely. Only molecules carrying sufficient internal energy would be able to stimulate the current reaction. Since all the electronically excited states of SiH_4 and Si_2H_6 are unstable and lead to immediate dissociation, this process is therefore not very probable.

Taking the above arguments in mind, the detachment of an electron from an anion seems not very likely in the present situation, and is therefore neglected in our simulations. Hence, only mutual anion-cation neutralization is taken into account as loss mechanism for the anions.

C. The plasma-wall interaction

A sticking model describes the plasma-wall interaction for each neutral species and makes sure that the loss of species due to deposition at the walls is taken into account. Although some preliminary information about the growth of the layer can be obtained from the model, we mainly focus our attention on the discharge itself. These boundary conditions, however, cannot be neglected, since they alter the plasma densities of the depositing species. The model assumes that only the radicals react with the surface, while the neutral molecules (SiH_4, Si_nH_{2n+2}, H_2) are reflected into the discharge. The decay of the vibrationally excited SiH_4 molecules at the walls is, however, incorporated by a 100% reaction chance in the surface reaction probability.

The surface reaction probability is composed of a probability for sticking of the radical on the surface and a probability for recombination of the radical at the surface to form, e.g., SiH_4 and Si_2H_6 with other species on the surface.

The SiH_3 radical is assumed to be the most dominant species contributing to the film growth [53]. The surface reaction coefficient of SiH_3 is considered temperature independent at a substrate temperature between room temperature and 750 K, and is set at 0.26 [31]. The surface sticking co-

efficient of SiH_3 is 0.09 [31], which means that a fraction of 0.17 recombines to SiH_4 at the surface. Likewise, a silyl radical (Si_nH_{2n+1}) can recombine with a hydrogen atom at the surface and is emitted as Si_nH_{2n+2} into the discharge. Because the structure of Si_nH_{2n+1} radicals, for $n>1$, is similar to that of SiH_3, the same surface reaction coefficients are used [43]. For SiH_2 the sticking coefficient is set at 0.8 [43]. Radicals that are assumed to be responsible for film growth are SiH_3, SiH_2, and Si_2H_5 and their sticking coefficients are set at 0.09, 0.8, and 0.09, respectively, bearing in mind that the concentration of SiH_2 is extensively diminished by the SiH_2 insertion reactions described in Table III (reactions 5–7).

Information about surface reaction coefficients of larger clusters is unavailable in literature, hence some approximations had to be made. Because the structure of silylenes somewhat relates to that of SiH_2, the same sticking coefficients are used. A sensitivity study showed, however, that by altering the sticking coefficients of silylenes, their density in the plasma bulk remains nearly unaffected, which is here of primary concern.

Positive ions can also be incorporated into the growing film and their sticking coefficient is assumed to be equal to one. Anions, however, are unable to reach the reactor boundaries, so they do not play a direct role as depositing species.

When a Si_nH_m radical sticks to the surface, not all hydrogen is deposited in the layer. Only 10% of the hydrogen will be incorporated into the layer, while the rest of the hydrogen will flow back to the plasma as molecular hydrogen. Hence, when a radical is adsorbed, this process is immediately followed by an adequate amount of H_2 desorption from the surface.

D. The transport of species in the plasma

The diffusion coefficient D_j (m^2/s) of a neutral molecule j in a background mixture of SiH_4, H_2, and Si_2H_6 gas is obtained by first determining the separate diffusion coefficients in each of the background gases i (SiH_4, Si_2H_6, and H_2) from the classical expression for binary collisions [43],

$$D_{ij} = \frac{3}{16}\frac{k_B T_{gas}}{p_{tot}}\frac{(2\pi k_B T_{gas}/m_r)^{1/2}}{\pi\sigma_{ij}^2\,\Omega_D(\Psi)}, \tag{26}$$

where k_B is the Boltzmann constant, T_{gas} is the gas temperature in kelvin, m_r is the reduced mass in amu, $\sigma_{ij}=(\sigma_i+\sigma_j)/2$ is the binary collision diameter in Å, P_{tot} is the total pressure in pascal units, and $\Omega_D(\Psi)$ is the diffusion collision integral with $\Psi=T/\epsilon_{ij}$ and $\epsilon_{ij}=(\epsilon_i+\epsilon_j)^{0.5}$. The Lennard-Jones parameters ϵ_j and σ_j, in eV and Å, respectively, are obtained from Ref. [43]. The diffusion coefficient D_j of species j in the background gas mixture can then be approximated using Blancs law [54],

$$\frac{p_{tot}}{D_j} = \sum_{i=\text{background gases}} \frac{p_i}{D_{ij}}. \tag{27}$$

We can conclude from Eq. (26) that D_j decreases with cluster size.

For the calculation of the ion mobility coefficients a similar procedure is used. The ion mobility of ion j in background neutral i (in $m^2\ V^{-1}\ s^{-1}$) is calculated using the low E-field Langevin mobility expression [54],

$$\mu_{ij} = 0.514 m_r^{0.5}\frac{T_{gas}}{p_{tot}}\alpha_i^{-0.5}, \tag{28}$$

where the reduced mass m_r is in amu and the polarizability of the gas molecule i (α_i) is in $Å^3$. The ion mobility μ_j in the background gas mixture is again obtained using Blancs law.

The ion diffusion coefficient can be derived from the ion mobility via the Einstein relationship,

$$D_j^{\pm} = \frac{k_B T_{ion}}{e}\mu_j, \tag{29}$$

where T_{ion} is the ion temperature, which is assumed to be equal to the gas temperature T_{gas}. The expression of the ion mobility shows that μ_j, and hence also $D_j^{\pm}$, decrease with cluster size as well.

III. RESULTS AND DISCUSSION

In this section the results obtained from the 1D calculations are presented and discussed. All simulations were carried out for a parallel-plate, capacitively coupled radio frequency discharge, for a pressure of 40 Pa and a power of 5 W. These are typical conditions for which dust formation takes place [31]. The electrode gap is set at 3 cm. One electrode is connected to the power supply with a driving frequency of 50 MHz,while the other is electrically grounded. In order to investigate the temperature dependence the gas temperature will be varied between 293 K and 500 K at the end of this section, but for all other simulations it is kept constant at 400 K. In all calculations the silane gas flow is set at 20 SCCM (SCCM—cubic centimeter per minute at STP). A rate constant of $10^{-18}\ m^3\ s^{-1}$ (k_{g2}) for ground state SiH_4–anion reactions is adopted, unless indicated otherwise. In Sec. III B the variation of the anion-neutral reactions (between $k_{g1}=10^{-16}\ m^3\ s^{-1}$ and $k_{g2}=10^{-18}\ m^3\ s^{-1}$) will be investigated.

No secondary electrons are taken into account, so the results are limited to the α regime of a capacitively coupled radio frequency discharge, which is a valid assumption for the conditions under consideration [55,56]. The time step of a rf cycle in the model is equal to 2.5×10^{-10} s. A longer time step of 10^{-5} s is adopted for the description of the neutral-neutral chemistry to speed up the calculation.

A. Standard model

Figure 2 presents the calculated density profiles of the positive ions and electrons (a), and the anions (b) at the discharge conditions described above. In the bulk of the discharge the electric field is weak, but strong electric fields are present in the sheaths. Therefore, some variation of the ion density and especially of the electron density can occur in the sheaths, but we show here time-averaged electron and ion densities.

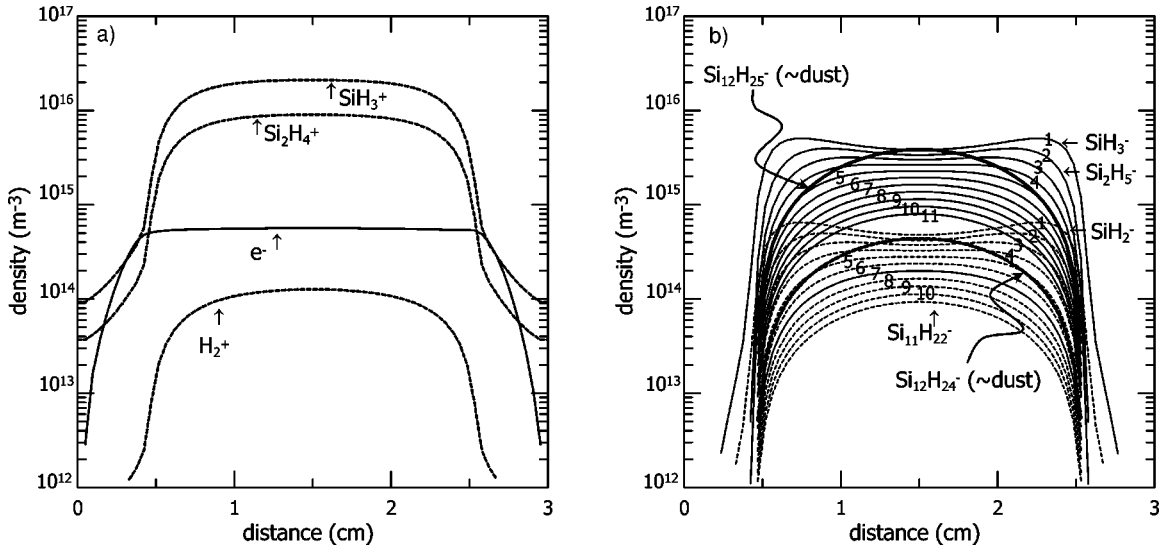

FIG. 2. Calculated density profiles of the ions and electrons (assuming $k_{g2}=10^{-18}$ m^3 s^{-1}) (a) positive ions and electrons; (b) anions.

The major positive ion appears to be SiH_3^+ with a density of about 2×10^{16} m^{-3} in the center of the discharge [see Fig. 2(a)]. The density of $Si_2H_4^+$ is approximately two times lower (at maximum 9×10^{15} m^{-3}). Note that the H_2^+ density is more than two orders of magnitude lower, as H_2^+ is only produced by electron impact collisions on H_2 above 15.4 eV (see Fig. 1), and hence it is only considered as a minor product. Consequently, no ion-ion neutralization reactions have to be included for H_2^+ (see above, Sec. II). The electron density is almost two orders of magnitude lower than the positive ion density due to the presence of the anions and it is of the order of 5×10^{14} m^{-3} in the plasma bulk.

For the sake of clarity the negative ions are plotted separately in Fig. 2(b). The SiH_4 discharge is a typical electronegative plasma, resulting in a high negative ion density in comparison to the electron density. Indeed, the electron density in the plasma bulk is about 7.5 times less than the density of the most dominant anion because of the electron loss by attachment. Two different pathways, starting from either SiH_3^- or SiH_2^-, can be distinguished and lead to, respectively, the growth of larger silyl ($Si_nH_{2n+1}^-$) and silylene ($Si_nH_{2n}^-$) anions, due to successive polymerization reactions. The number indicated on each density profile specifies the number of silicon atoms, n, and indirectly the number of hydrogen atoms ($2n+1$ for silyl and $2n$ for silylene anions). In order to differentiate between both types of anions, the silylene anions (starting from SiH_2^-) are represented by a dashed line. A gradually decreasing trend of the anion density can be observed as the number of silicon atoms increases. This is in good agreement with the experimental results obtained by Howling *et al.* [28], where the same trend is detected in their mass spectrometric measurements. This decrease can be attributed to the fact that a larger anion, containing n silicon atoms, is produced by the reaction of SiH_4 with an anion containing $n-1$ silicon atoms. As the polymerization path continues, every previous anion is also lost due to the mutual neutralization reactions, leading to a lower production of the succeeding anion. Both pathways are stopped in the model at anions containing 12 silicon atoms, leading to the formation of $Si_{12}H_{25}^-$ and $Si_{12}H_{24}^-$, respectively. Note that the density of $Si_{12}H_{25}^-$ and $Si_{12}H_{24}^-$ is about one order of magnitude higher than the density of the corresponding smaller anions in the same pathway. This can be explained by the fact that both species do not undergo further polymerization reactions, and hence are only lost due to mutual neutralization with either SiH_3^+ or $Si_2H_4^+$. Therefore, these species can be considered as dust, as they symbolize the sum of all bigger anions present in the discharge. Hence, we can conclude from Fig. 2(b) that SiH_3^- is calculated to be the main precursor of the dust formation, as the silyl pathway appears to be much more important in comparison to the silylene pathway. Over 90% of the particle formation proceeds through the silyl pathway and hence mainly $Si_{12}H_{25}^-$ is formed.

The densities of the most important molecules and radicals are shown in Figs. 3 and 4, respectively. Species reacting at the surface are characterized by their decreasing density towards the electrodes. The densities of the background neutrals (SiH_4, H_2, and Si_nH_{2n+2} with $n\geqslant2$) are homogeneously distributed over the entire reactor. The background gas SiH_4 is present at the highest density, and takes a value of about 4×10^{21} m^{-3}. Opposed to ground state SiH_4, the density profiles of the vibrationally excited SiH_4 molecules ($SiH_4^{(2-4)}$ and $SiH_4^{(1-3)}$) decrease near the electrodes, representing their decay at the wall to ground state SiH_4, which is incorporated by a 100% reaction probability. The $SiH_4^{(2-4)}$ and $SiH_4^{(1-3)}$ profiles reach a concentration of about 5×10^{18} m^{-3} and 4×10^{18} m^{-3} in the plasma bulk, respectively, meaning that their density is around three orders of magnitude lower than the ground state SiH_4 density. The H_2 density, at 2.5×10^{21} m^{-3}, is relatively high. This is due to a large number of reactions in Table IV which lead to the production of H_2. Furthermore, the sticking of a radical on the surface causes the reflection of H_2 into the discharge, as was explained above. Higher order silane molecules are formed by SiH_2 insertion reactions (reactions 5–7 in Table III) and show, similar to the anion density profiles, a decreasing trend towards higher silicon hydrides. The density of the

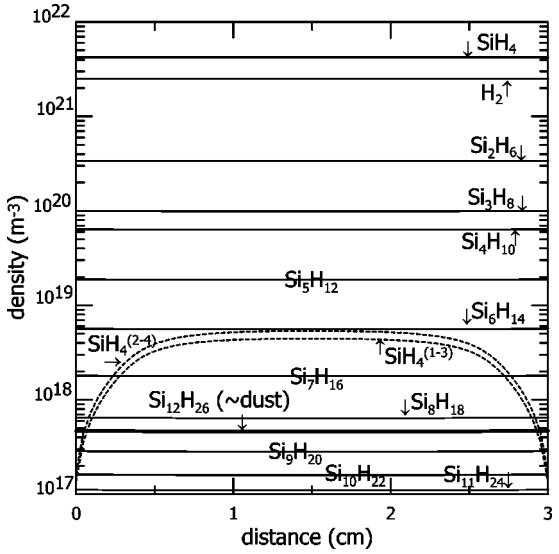

FIG. 3. Calculated density profiles of the Si_nH_{2n+2} molecules and the first vibrational levels $SiH_4^{(2-4)}$ and $SiH_4^{(2-3)}$ (assuming $k_{g2} = 10^{-18}$ m^3 s^{-1}).

highest neutral, $Si_{12}H_{26}$, is slightly higher, since no SiH_2 insertion reaction is incorporated, as loss mechanism. Hence, $Si_{12}H_{26}$ is only lost due to pumping in the reactor.

From Fig. 4 we can conclude that the most important radical in the plasma is SiH_3 with a density at the maximum of its profile of about 3×10^{18} m^{-3}. A distinction is made between the silyl radicals (Si_nH_{2n+1}) and the silylenes (Si_nH_{2n}), the latter being characterized by a dashed line. The silylene radicals appear to have the lowest density. They are only included in our model because their respective silylene anions are important in propagating the clustering process. The silylenes, containing 2 to 12 silicon atoms, attain approximately equal concentrations, since they are only produced by mutual neutralization reactions, which proceed at nearly the same rate constant for all cluster sizes (see Table IV). Hence, their densities are represented by several indicative lines with the notation Si_nH_{2n}. Only SiH_2 is produced at a much higher rate, given that the dissociation of SiH_4 mainly leads to the production of SiH_2 (see above: Fig. 1 and Table II).

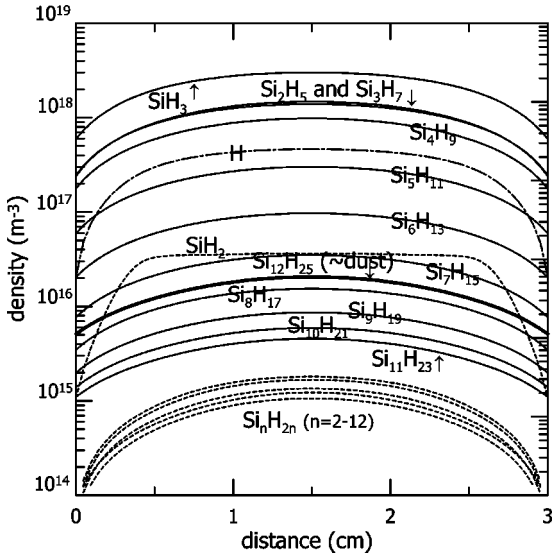

FIG. 4. Calculated density profiles of the silyl radicals Si_nH_{2n+1} and the silylenes Si_nH_{2n} (assuming $k_{g2} = 10^{-18}$ m^3 s^{-1}).

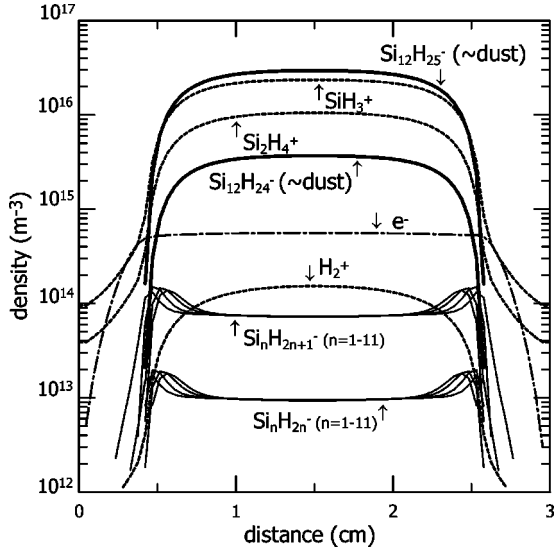

FIG. 5. Calculated density profiles of the positive and negative ions and electrons (assuming $k_{g1} = 10^{-16}$ m^3 s^{-1}).

B. Effect of variation of anion-molecule rate constants

Exact data for the actual rate constants of the anion-molecule clustering reactions are still not known. To evaluate the sensitivity of the model predictions with respect to these anion-SiH_4 rate constants, calculations have been performed where the anion-SiH_4 rate constants are varied between the two values assumed in literature, i.e., 10^{-18} m^3 s^{-1} (k_{g_2}), which is adopted in our standard model, and 10^{-16} m^3 s^{-1} (k_{g1}), taken from the Langevin rate constant but reduced by an order of magnitude (see above).

In Fig. 5 the time-averaged ion density profiles for an anion–ground state rate constant of 10^{-16} m^3 s^{-1} are shown. In this case the cluster growth through both vibrationally excited SiH_4 molecules will proceed at the maximum rate of 10^{-15} m^3 s^{-1} (i.e., the Langevin rate). Figure 5 shows that the density profiles of the anions differ significantly from the profiles depicted in the standard model. The silyl and the silylene anions containing 1 to 11 silicon atoms reach approximately equal concentrations within each pathway, and are therefore represented by the notation $Si_nH^-_{2n+1}$ and $Si_nH^-_{2n}$, respectively. The buildup of dust species is much more substantial (of the order of 3×10^{16} m^{-3} for the $Si_{12}H^-_{25}$ density, in comparison with 4×10^{15} m^{-3} in the standard model), since the anion-neutral reactions proceed at a much faster rate, leading to lower concentrations of the intermediate negative ions. Therefore, $Si_{12}H^-_{25}$ and $Si_{12}H^-_{24}$ reach a density which is about two orders of magnitude higher than the densities of the corresponding smaller anions in the same pathway. Unlike the standard model, local maxima appear at the bulk-sheath boundary of the anions profile and a local

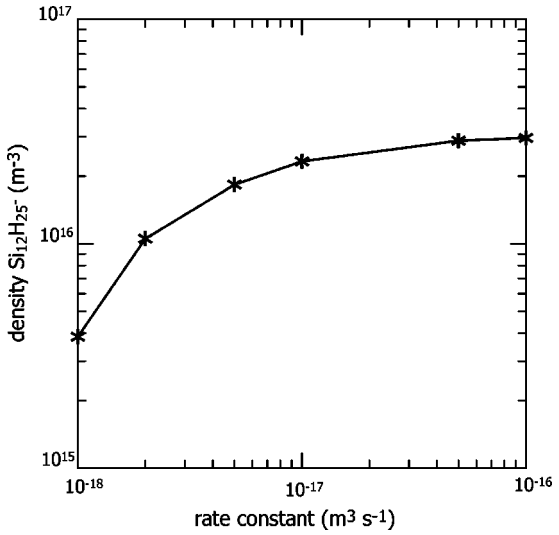

FIG. 6. Calculated variation of the density of $Si_{12}H_{25}^-$ as a function of the assumed anion-silane clustering rate constant.

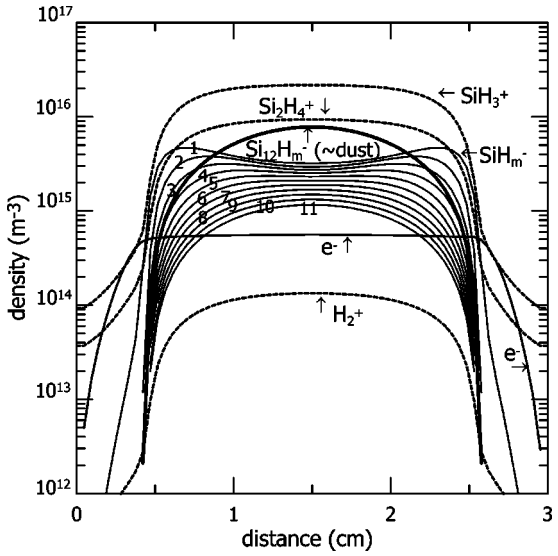

FIG. 7. Calculated density profiles of the positive and negative ions and electrons (assuming $k_{g2}=10^{-18}$ m^3 s^{-1}), when also SiH_3-anion reactions are included in the model.

minimum is obtained in the center of the discharge. This minimum can be attributed to the very fast mutual neutralization, which mainly occurs in the plasma bulk, where the densities of the positive ions reach a maximum. Similar importance of the different pathways is maintained, as SiH_3^- still remains the most important precursor of the dust formation and 90% of the clustering reactions propagate through the silyl pathway. In contrast to the changes of the anion density profiles, the positive ion and electron distributions remain similar to the ones of the standard model. Hence, the total sum of the negative ions remains the same.

Figure 6 shows the calculated density of $Si_{12}H_{25}^-$ in the plasma bulk as a function of assumed anion-SiH_4 clustering rate constant. Note that increasing the rate constants of the anion–ground state SiH_4 reactions in the discharge from k_{g2} to k_{g1} enhances the density of $Si_{12}H_{25}^-$ by a factor of 7.5. This shows that the clustering rate constant can indeed influence the buildup of the dust considerably.

C. Effect of anion-radical reactions

In order to assess the role of the anion-radical reactions we have to make some changes to the standard model. If we include reactions between the anions and the radicals, no distinction can be made between the silyl and the silylene anions, since, as was explained above, the modeling of the discharge would become a tedious procedure. Therefore, the particle formation starts from SiH_m^- with m comprising anions having three to zero hydrogen atoms. Only reactions between anions and the most abundant radical, SiH_3, have been included, at a rate constant of 10^{-15} m^3 s^{-1} [27]. Reactions with larger radicals (Si_nH_{2n+1} with $n>1$) are not taken into account, because of their lower densities (see Fig. 4), thus making their contribution less effective. A reaction rate constant of 10^{-18} m^3 s^{-1} (k_{g2}) has been adopted for the anion-SiH_4 reactions in this case.

Figure 7 shows the calculated density profiles of the ions. The number on each density plot specifies the number of silicon atoms. The structure of the density profiles is similar to that of the standard model. By introducing the anion-radical reactions, the density of the largest species $Si_{12}H_m^-$, which can be seen as a summation of the $Si_{12}H_{25}^-$ and $Si_{12}H_{24}^-$ densities of the standard model, increases in comparison with the standard model by a factor of 1.8. This implies that at the rate constant k_{g2}, the radicals will help to propagate the clustering chain (see below). No change can be observed in the density profile of electrons and the positive ions.

The relative importance of the radicals and that of the vibrationally excited SiH_4 molecules is discussed in the following paragraph.

D. Role of vibrationally excited silane molecules and SiH_3 radicals

The contribution of the vibrationally excited silane molecules SiH_4^* (i.e., $SiH_4^{(2-4)}$ and $SiH_4^{(1-3)}$) and of the SiH_3 radicals will depend on the actual clustering rate constant of the anion – ground state SiH_4 reactions. As can be seen from the standard model (see Figs. 3 and 4), the SiH_4^* and SiH_3 densities are about three orders of magnitude lower than the SiH_4 density, meaning that the reactivity of the anions towards SiH_4^* and SiH_3 has to be much higher than their reactivity towards SiH_4 in order for these mechanisms to be important.

Figure 8 shows the relative contribution of the different anion reaction pathways as a function of the assumed anion-SiH_4 clustering rate constant. At a rate constant of 10^{-18} m^3 s^{-1}, about 38% of the anions react with SiH_4 ground state molecules, 36% of the anions proceed through the $SiH_4^{(1-3)}$ pathway, and over 25% react with SiH_3 radicals. With 1.2% the $SiH_4^{(2-4)}$ contribution is of minor importance. By increasing the anion–ground state SiH_4 reaction rate constant from k_{g2} (10^{-18} m^3 s^{-1}) to k_{g1} (10^{-16} m^3 s^{-1}), the contribution of the SiH_3 radicals will drop rapidly to less than

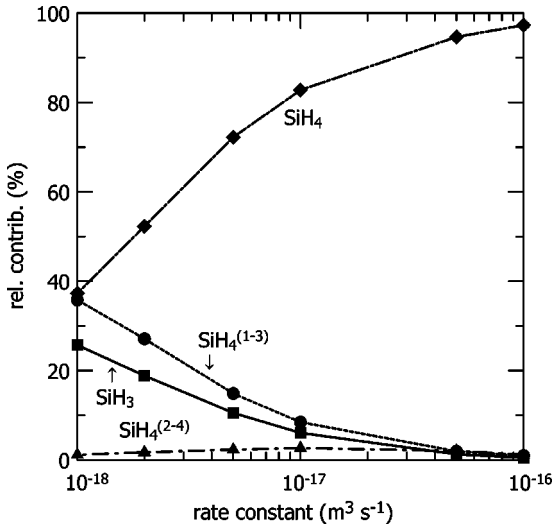

FIG. 8. Calculated relative contributions of the different anion reaction pathways as a function of the assumed ground state silane clustering rate constant.

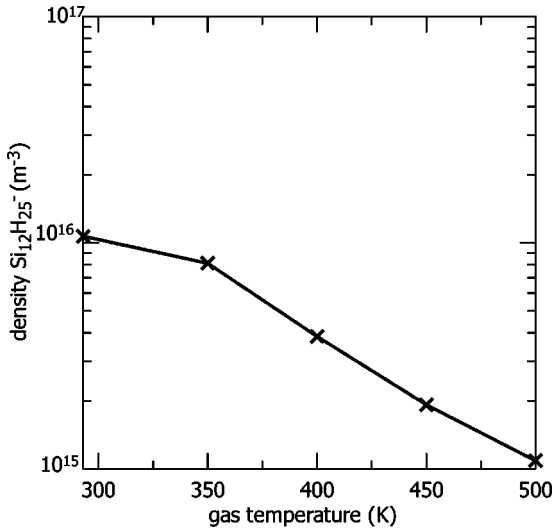

FIG. 9. Variation of the calculated density of $Si_{12}H_{25}^-$ anions as a function of gas temperature.

1%, as the SiH_3 radicals, propagating the clustering process at a rate constant of 10^{-15} m^3 s^{-1}, become less important on a relative scale. Similarly, the contribution of the vibrationally excited species, $SiH_2^{(2-4)}$ and especially that of $SiH_4^{(1-3)}$, will decrease. This can be explained by the fact that the rate constants of anion-SiH_4^* reactions can never exceed the Langevin rate constant. Hence, as the rate constant of ground state SiH_4 is increased, the rate constant of the SiH_4^* remains at its maximum value of 10^{-15} m^3 s^{-1}.

We can conclude from Fig. 8 that depending on the actual rate constant of the anion – ground state SiH_4 reactions, the SiH_4^* and SiH_3 will or will not play an important role in the clustering process. But if, as suggested by several authors [57], the vibrationally excited SiH_4^* molecules help to drive the polymerization pathway, the clustering rate constant for the ground state should be in any case lower than 10^{-16} m^3 s^{-1}.

E. Variation of gas temperature

The influence of the gas temperature on particle formation is demonstrated in Fig. 9, where the density of the largest anion considered in this work ($Si_{12}H_{25}^-$) is plotted as a function of gas temperature. The concentration of $Si_{12}H_{25}^-$ refers to that at the center of the discharge. Calculations have been performed for five different gas temperatures ranging between ambient temperature and 500 K. To account for the influence of the temperature dependence in our model, the mobility and diffusion coefficient of every species is recalculated at each given temperature T (in kelvin). Reaction rate constants that involve a temperature dependence are also readjusted to the specific temperature T. These include the hydrogen abstraction (reactions 1–4), shown in Table III, and the cluster growth through vibrationally excited SiH_4 (reactions 2–3 and 5–6), deexcitation of vibrationally excited SiH_4 (reactions 7–10), and neutralization of negative ions with SiH_3^+ and $Si_2H_4^+$ (reactions 11–14), all shown in Table IV.

From Fig. 9 we can conclude that variations in the gas temperature have a significant effect on the growth of dust species, as an increase in the gas temperature results in a decrease of the $Si_{12}H_{25}^-$ density. Although, in our present model no coagulation of the clusters is described yet, we can conclude from these results that a lower anion density at higher gas temperatures indicates that the growth of dust particles will be delayed. Indeed, a lower production of the smaller species, here mostly $Si_{12}H_{25}^-$, will lead to a longer buildup time of the dust. This concurs with the experimental results, where the appearance of nanometer sized dust particles is delayed at higher gas temperatures. At room temperature small particles appear almost immediately (i.e., after a few milliseconds), while at 500 K it will take more than 10 s after ignition of the rf discharge before some dust particles are observed [58].

Several possible explanations for the delay of particle nucleation have been proposed [49] (and references cited herein). The production of SiH_3^- and SiH_2^- through electron impact dissociative attachment on SiH_4, appears to be temperature independent in the experiments performed by Boufendi [59]. On the other hand, especially the succeeding polymerization reactions, starting from either SiH_3^- or SiH_2^-, are influenced by adjusting the gas temperature [59]. From our calculations we deduce that both the temperature dependence of the mobility and diffusion coefficients, as well as the deexcitation of the vibrationally excited SiH_4 will probably play a role. As mentioned in the previous paragraph, at 400 K and a clustering rate constant k_{g2} (which is adopted in all temperature dependent calculations) over 36% of the clustering reactions proceed through the vibrationally excited pathway. It is well known that at increased gas temperatures, gas collisions become more important, hence, the deexcitation of the vibrationally excited SiH_4 molecules becomes much more efficient. Moreover, by increasing the gas temperature, the rate constants of anion-SiH_4^* will decrease [see Eq. (14)]. Both mechanisms will thus lead to a smaller contribution of the vibrationally excited species to the propagation of the dust formation, hence, a delay can occur.

IV. SUMMARY AND CONCLUSIONS

A one-dimensional fluid model has been developed to describe the mechanisms of particle formation in a low-pressure SiH_4 discharge. The model includes 68 different species and the formation of silicon hydrides containing up to a maximum of 12 silicon atoms is incorporated. Several gas-phase reactions leading to the formation of larger clusters have been discussed. The anions play a crucial role in the dust formation, as anion-silane reactions drive the polymerization pathway.

From the standard model it was found that the anion SiH_3^- is the most dominant primary precursor of the particle formation. We conclude that over 90% of the dust formation proceeds through the silyl anion ($Si_nH_{2n+1}^-$) pathway, starting from SiH_3^-, and only about 10% through the silylene anion ($Si_nH_{2n}^-$) pathway, starting from SiH_2^-.

The effect of variation of particle growth rate constants and of the gas temperature on the density of the dust particles was investigated. A variation of the particle growth rate constants from 10^{-18} m^3 s^{-1} to 10^{-16} m^3 s^{-1} resulted in a significant change of the anion density profiles, but the relative importance of the different pathways remained the same. The role of the vibrationally excited silane molecules ($SiH_4^{(2-4)}$ and $SiH_4^{(1-3)}$) and of the SiH_3 radicals will depend on the exact rate constant of the anion–ground state SiH_4 reactions, which is *a priori* not exactly known. However, we can conclude that, if the vibrationally excited silane molecules are important in propagating the reaction pathway, the reaction rate constant of anion–ground state SiH_4 should be clearly less than 10^{-16} m^3 s^{-1}.

Finally we have observed a decrease in the dust density when the gas temperature is increased, meaning that a delay in the nucleation of the particle formation takes place, as is also seen in experiments.

ACKNOWLEDGMENTS

K. De Bleecker is indebted to the Institute for the Promotion of Innovation through Science and Technology in Flanders (IWT-Vlaanderen) for financial support. A.B. acknowledges financial support from the Flemish Fund for Scientific Research (FWO). This work was also supported by the Belgian Federal Services for Scientific, Technical and Cultural Affairs of the Prime Minister's Office through IUAP-V. The authors wish to thank Dr. U. Bhandarkar for very stimulating discussions.

[1] M. J. Kushner, J. Appl. Phys. **63**, 2532 (1988).
[2] A. Grill, *Cold Plasma in Materials Fabrication: From Fundamentals to Applications* (IEEE Press, New York, 1994).
[3] C. Koch, M. Ito, and M. Schubert, Sol. Energy Mater. Sol. Cells **68**, 227 (2001).
[4] B. Chapman, *Glow Discharge Processes* (Wiley, New York, 1980).
[5] A. H. Mahan, J. Carapella, B. P. Nelson, R. S. Crandall, and I. Balberg, J. Appl. Phys. **69**, 6728 (1991).
[6] S. Will, H. Mell, M. Poschenrieder, and W. Fuhs, J. Non-Cryst. Solids **227-230**, 29 (1998).
[7] O. Saadame, C. Longeaud, S. Lebib, and P. Roca i Cabarrocas, Thin Solid Films **427**, 241 (2003).
[8] Y. Kuo, K. Okajima, and M. Takeichi, IBM J. Res. Dev. **43**, 73 (1999).
[9] J. L. Crowley, Solid State Technol. **35**, 94 (1992).
[10] Ph. M. Fauchet, J. Lumin. **80**, 53 (1998).
[11] J. Kocka, I. Pelant, and A. Fejfar, J. Non-Cryst. Solids **198-200**, 57 (1996).
[12] G. S. Selwyn, J. Singh, and R. S. Benett, J. Vac. Sci. Technol. A **7**, 2758 (1989).
[13] A. Bouchoule, in *Dusty Plasmas: Physics, Chemistry and Technological Impacts in Plasma Processing*, edited by A. Bouchoule (Wiley, Chichester, UK, 1999).
[14] P. Roca i Cabarrocas, S. Hamma, S. N. Sharma, G. Viera, E. Bertran, and J. Costa, J. Non-Cryst. Solids **227-230**, 871 (1998).
[15] C. Longeaud, J. P. Kleider, P. Roca i Cabarrocas, S. Hamma, R. Meaudre, and C. Meaudre, J. Non-Cryst. Solids **227-230**, 96 (1998).
[16] M. Meaudre, R. Meaudre, R. Butté, and S. Vignoli, J. Appl. Phys. **86**, 946 (1999).
[17] A. Fontcuberta i Morral, Ph.D. thesis, École Polytechnique de France, 2001 (unpublished).
[18] W. W. Stoffels and E. Stoffels, Trends Vac. Sci. Technol. **4**, 1 (2001).
[19] A. Gallagher, Phys. Rev. E **62**, 2690 (2000).
[20] A. Gallagher, A. A. Howling, and Ch. Hollenstein, J. Appl. Phys. **91**, 5571 (2002).
[21] U. V. Bhandarkar, M. T. Swihart, S. L. Girshick, and U. R. Kortshagen, J. Phys. D **33**, 2731 (2000).
[22] P. M. Meijer, Ph.D. thesis, Utrecht University, 1991 (unpublished).
[23] K. De Bleecker, A. Bogaerts, W. Goedheer, and R. Gijbels, IEEE Trans. Plasma Sci. (to be published).
[24] M. L. Mandich, W. D. Reents, Jr., and K. D. Kolenbrander, J. Chem. Phys. **92**, 437 (1990).
[25] Y. Watanabe, M. Shiratani, T. Fukuzawa, H. Kawasaki, Y. Ueda, S. Singh, and H. Ohkura, J. Vac. Sci. Technol. A **14**, 995 (1996).
[26] T. Fukuzawa, K. Obata, H. Kawasaki, M. Shiratani, and Y. Watanabe, J. Appl. Phys. **80**, 3202 (1996).
[27] J. Perrin, C. Böhm, R. Etemadi, and A. Lloret, Plasma Sources Sci. Technol. **3**, 252 (1994).
[28] A. A. Howling, L. Sansonnens, J.-L. Dorrier, and Ch. Hollenstein, J. Phys. D **26**, 1003 (1993).
[29] C. Courteille, J.-L. Dorier, Ch. Hollenstein, L. Sansonnens, and A. A. Howling, Plasma Sources Sci. Technol. **5**, 210 (1996).
[30] Ch. Hollenstein, J.-L. Dorier, J. Dutta, L. Sansonnens, and A. A. Howling, Plasma Sources Sci. Technol. **3**, 278 (1994).
[31] G. J. Nienhuis, W. J. Goedheer, E. A. G. Hamers, W. G. J. H.

M. van Sark, and J. Bezemer, J. Appl. Phys. **82**, 2060 (1997).
[32] G. J. Nienhuis, Ph.D. thesis, Utrecht University, 1998.
[33] J. D. P. Passchier, Ph.D. thesis, Utrecht University, 1994.
[34] J. D. P. Passchier and W. J. Goedheer, J. Appl. Phys. **73**, 1073 (1993).
[35] E. Krishnakumar and S. K. Srivastava, Contrib. Plasma Phys. **35**, 395 (1995).
[36] M. Kurachi and Y. Nakamura, J. Phys. D **22**, 107 (1989).
[37] J. Perrin, J. P. M. Schmitt, G. de Rosny, B. Drevillon, J. Huc, and A. Lloret, Chem. Phys. **73**, 383 (1982).
[38] J. R. Doyle, D. A. Doughty, and A. Gallagher, J. Appl. Phys. **68**, 4375 (1990).
[39] P. Haaland, J. Chem. Phys. **93**, 4066 (1990).
[40] H. Tawara and T. Kato, At. Data Nucl. Data Tables **36**, 167 (1987).
[41] H. Ehrhardt, L. Langhans, F. Linder, and H. S. Taylor, Phys. Rev. **173**, 222 (1968).
[42] A. G. Engelhardt and A. V. Phelps, Phys. Rev. **131**, 2115 (1963).
[43] J. Perrin, O. Leroy, and M. C. Bordage, Contrib. Plasma Phys. **36**, 3 (1996).
[44] E. Krishnakumar and S. K. Srivastava, Int. J. Mass Spectrom. Ion Processes **103**, 107 (1990).
[45] J. M. Wadehra and J. N. Bardsley, Phys. Rev. Lett. **41**, 1795 (1978).
[46] L. G. Christophorou, Environ. Health Perspect. **36**, 3 (1980).
[47] E. R. Austin and F. W. Lampe, J. Phys. Chem. **81**, 1134 (1977).
[48] N. Itabashi, K. Kato, N. Nishiwaki, T. Goto, C. Yamada, and E. Hirota, Jpn. J. Appl. Phys., Part 2 **28**, L325 (1989).
[49] U. Bhandarkar, U. Kortshagen, and S. L. Girshick, J. Phys. D **36**, 1399 (2003).
[50] A. P. Hickman, J. Chem. Phys. **70**, 4872 (1979).
[51] A. A. Fridman, L. Boufendi, T. Hbid, B. V. Potapkin, and A. Bouchoule, J. Appl. Phys. **79**, 1303 (1996).
[52] M. T. Swihart, J. Phys. Chem. A **104**, 6083 (2000).
[53] J. Perrin, M. Shiratani, P. Kae-Nune, H. Videlot, J. Jolly, and J. Guillon, J. Vac. Sci. Technol. A **16**, 278 (1998).
[54] E. W. McDaniel and E. A. Mason, *The Mobility and Diffusion of Ions in Gases* (Wiley, New York, 1973).
[55] Ph. Belenguer and J. P. Boeuf, Phys. Rev. A **41**, 4447 (1990).
[56] M. Surendra and D. B. Graves, IEEE Trans. Plasma Sci. **19**, 144 (1991).
[57] J. Perrin and Ch. Hollenstein, in *Dusty Plasmas: Physics, Chemistry and Technological Impacts in Plasma Processing*, edited by A. Bouchoule (Wiley, Chichester, UK, 1999).
[58] L. Boufendi, J. Hermann, A. Bouchoule, B. Dubreuil, E. Stoffels, W. W. Stoffels, and M. L. de Giorgi, J. Appl. Phys. **76**, 148 (1994).
[59] L. Boufendi (private communication).